Thermal noise in mid-infrared broadband upconversion detectors

Barh, Ajanta; Tidemand-Lichtenberg, Peter; Pedersen, Christian

Published in:
Optics Express

Link to article, DOI:
10.1364/OE.26.003249

Publication date:
2018

Document Version
Publisher's PDF, also known as Version of record

Research Article | Vol. 26, No. 3 | 5 Feb 2018 | OPTICS EXPRESS 3249
Optics EXPRESS

Thermal noise in mid-infrared broadband upconversion detectors

AJANTA BARH,* PETER TIDEMAND-LICHTENBERG, AND CHRISTIAN PEDERSEN

DTU Fotonik, Technical University of Denmark, DK-4000 Roskilde, Denmark
**ajaba@fotonik.dtu.dk*

Abstract: Low noise detection with state-of-the-art mid-infrared (MIR) detectors (e.g., PbS, PbSe, InSb, HgCdTe) is a primary challenge owing to the intrinsic thermal background radiation of the low bandgap detector material itself. However, researchers have employed frequency upconversion based detectors (UCD), operable at room temperature, as a promising alternative to traditional direct detection schemes. UCD allows for the use of a low noise silicon-CCD/camera to improve the SNR. Using UCD, the noise contributions from the nonlinear material itself should be evaluated in order to estimate the limits of the noise-equivalent power of an UCD system. In this article, we rigorously analyze the optical power generated by frequency upconversion of the intrinsic black-body radiation in the nonlinear material itself due to the crystals residual emissivity, i.e. absorption. The thermal radiation is particularly prominent at the optical absorption edge of the nonlinear material even at room temperature. We consider a conventional periodically poled lithium niobate (PPLN) based MIR-UCD for the investigation. The UCD is designed to cover a broad spectral range, overlapping with the entire absorption edge of the PPLN (3.5 – 5 μm). Finally, an upconverted thermal radiation power of ~30 pW at room temperature (~30°C) and a maximum of ~70 pW at 120°C of the PPLN crystal are measured for a CW mixing beam of power ~60 W, supporting a good quantitative agreement with the theory. The analysis can easily be extended to other popular nonlinear conversion processes including OPO, DFG, and SHG.

OCIS codes: (190.7220) Upconversion; (190.4410) Nonlinear optics, parametric processes; (160.4330) Nonlinear optical materials; (120.6810) Thermal effects.

References and links

1. S. D. Jackson, "Towards high-power mid-infrared emission from a fibre laser," Nat. Photonics **6**(7), 423–431 (2012).
2. J. S. Dam, P. Tidemand-Lichtenberg, and C. Pedersen, "Room-temperature mid-infrared single-photon spectral imaging," Nat. Photonics **6**(11), 788–793 (2012).
3. P. Tidemand-Lichtenberg, J. S. Dam, H. V. Andersen, L. Høgstedt, and C. Pedersen, "Mid-infrared upconversion spectroscopy," J. Opt. Soc. Am. B **33**(11), D28 (2016).
4. A. Sijan, "Development of military lasers for optical countermeasures in the mid-IR," in SPIE Europe Security + Defense 2009 (International Society for Optics and Photonics, 2009), p. 748304.
5. L. Labadie and O. Wallner, "Mid-infrared guided optics: a perspective for astronomical instruments," Opt. Express **17**(3), 1947–1962 (2009).
6. R. Petersen, U. Møller, I. Kubat, B. Zhou, S. Dupont, J. Ramsay, T. Benson, S. Sujecki, N. Abdel-Moneim, Z. Tang, D. Furniss, A. Seddon, and O. Bang, "Mid-infrared supercontinuum covering the 1.4-13.3 μm molecular fingerprint region using ultra-high NA chalcogenide step-index fibre," Nat. Photonics **8**(11), 830–834 (2014).
7. Y. Yao, A. J. Hoffman, and C. F. Gmachl, "Mid-infrared quantum cascade lasers," Nat. Photonics **6**(7), 432–439 (2012).
8. A. Schliesser, N. Picqué, and T. W. Hänsch, "Mid-infrared frequency combs," Nat. Photonics **6**(7), 440–449 (2012).
9. A. Aadhi and G. K. Samanta, "High power, high repetition rate, tunable broadband mid-IR source based on single-pass optical parametric generation of a femtosecond laser," Opt. Lett. **42**(15), 2886–2889 (2017).
10. W. H. Kim, V. Q. Nguyen, L. B. Shaw, L. E. Busse, C. Florea, D. J. Gibson, R. R. Gattass, S. S. Bayya, F. H. Kung, G. D. Chin, R. E. Miklos, I. D. Aggarwal, and J. S. Sanghera, "Recent progress in chalcogenide fiber technology at NRL," J. Non-Cryst. Solids **431**, 8–15 (2016).
11. A. Rogalski, Infrared Detectors, 2nd ed. (CRC Press, 2011).

#312778 https://doi.org/10.1364/OE.26.003249
Journal © 2018 Received 7 Nov 2017; revised 25 Jan 2018; accepted 25 Jan 2018; published 30 Jan 2018

Optics EXPRESS

12. https://www.vigo.com.pl/products/infrared-detectors
13. F. Marsili, V. B. Verma, J. A. Stern, S. Harrington, A. E. Lita, T. Gerrits, I. Vayshenker, B. Baek, M. D. Shaw, R. P. Mirin, and S. W. Nam, "Detecting single infrared photons with 93% system efficiency," Nat. Photonics **7**(3), 210–214 (2013).
14. J. E. Midwinter, "Image conversion from 1.6 μ to the visible in lithium niobate," Appl. Phys. Lett. **12**(3), 68–70 (1968).
15. L. M. Kehlet, N. Sanders, P. Tidemand-Lichtenberg, J. S. Dam, and C. Pedersen, "Infrared hyperspectral upconversion imaging using spatial object translation," Opt. Express **23**(26), 34023–34028 (2015).
16. C. Pedersen, Q. Hu, L. Høgstedt, P. Tidemand-Lichtenberg, and J. S. Dam, "Non-collinear upconversion of infrared light," Opt. Express **22**(23), 28027–28036 (2014).
17. A. Barh, C. Pedersen, and P. Tidemand-Lichtenberg, "Ultra-broadband mid-wave-IR upconversion detection," Opt. Lett. **42**(8), 1504–1507 (2017).
18. S. Wolf, J. Kiessling, M. Kunz, G. Popko, K. Buse, and F. Kühnemann, "Upconversion-enabled array spectrometer for the mid-infrared, featuring kilohertz spectra acquisition rates," Opt. Express **25**(13), 14504–14515 (2017).
19. T. W. Neely, L. Nugent-Glandorf, F. Adler, and S. A. Diddams, "Broadband mid-infrared frequency upconversion and spectroscopy with an aperiodically poled LiNbO3 waveguide," Opt. Lett. **37**(20), 4332–4334 (2012).
20. G. Kirchhoff, "I. On the relation between the radiating and absorbing powers of different bodies for light and heat," Lond. Edinb. Dublin Philos. Mag. J. Sci. **20**, 1–21 (1860).
21. L. E. Estes, R. F. Lucy, J. Gunter, and K. Duval, "Internal thermal noise in optical frequency converters," J. Opt. Soc. Am. **64**(3), 295 (1974).
22. Y. C. See, S. Guha, and J. Falk, "Limits to the NEP of an intracavity $LiNbO_3$ upconverter," Appl. Opt. **19**(9), 1415–1418 (1980).
23. G. Temporão, S. Tanzilli, H. Zbinden, N. Gisin, T. Aellen, M. Giovannini, and J. Faist, "Mid-infrared single-photon counting," Opt. Lett. **31**(8), 1094–1096 (2006).
24. L. E. Myers, W. R. Bosenberg, R. C. Eckardt, M. M. Fejer, and R. L. Byer, "Multigrating quasi-phase-matched optical parametric oscillator in periodically poled LiNbO3," Opt. Lett. **21**(8), 591–593 (1996).
25. A. Barh, P. Tidemand-Lichtenberg, and C. Pedersen, "Concave grating enabled compact mid-IR upconversion spectrometer," in Proceedings of OSA Frontiers in Optics & Laser Science APS/DLS, Washington DC, USA, Sep. 2017 (oral).
26. R. L. Sutherland, Handbook of nonlinear optics (Second edition, Revised and Expanded, Marcel Dekker, Inc., 2003).
27. O. Gayer, Z. Sacks, E. Galun, and A. Arie, "Temperature and wavelength dependent refractive index equations for MgO-doped congruent and stoichiometric LiNbO3," Appl. Phys. B **91**(2), 343–348 (2008).
28. https://www.engineeringtoolbox.com/emissivity-coefficients-d_447.html

1. Introduction and background

Applications in the mid-infrared (MIR: 2 ~15 μm) wavelength range are numerous, ranging from precise molecular spectroscopy, food and pharmaceutical product analysis, soil contaminants and environmental monitoring, semiconductor processing, military applications, to astronomy [1–5]. Over the past decades, the MIR research community has grown fast with the advancement of high power, low noise narrow/broadband MIR sources [1, 6–9] as well as new optical materials [10]. Conversely, the growth of fast, low-noise, sensitive MIR detector technologies, particularly at room temperature, have constantly been hindered by inherent thermal noise in low bandgap materials (e.g. InSb, PbS or HgCdTe) at room temperature operation [11]. Thus research on MIR-detector is now propelling towards novel and unconventional techniques. Recently VIGO system [12] with room temperature operation has been commercialized; however, it is limited by speed. Superfast single-photon counting systems based on superconducting nanowire has been demonstrated at 1550 nm with very high efficiency (> 90%) [13]; however, it works only at extremely low temperature (≤ 2 K). With the demonstration of nonlinear frequency upconversion in the sixties [14], an alternative route of infrared detection was introduced. Recently a low noise MIR frequency upconversion based detector (UCD) at room temperature with a quantum efficiency of up to 20% has been successfully demonstrated [2]. Imaging [2, 15] and spectroscopy [3], narrowband [16] and broadband [17–19] UCDs have been demonstrated over substantial parts of the MIR range.

Upconversion is realized by mixing low energy photons (infrared) at wavelength λ_{IR} with pump photons at wavelength λ_p to generate upconverted photons of wavelength λ_{up}, under energy conservation and ideally the conservation of momentum

Optics EXPRESS

($\lambda_p^{-1} + \lambda_{IR}^{-1} = \lambda_{up}^{-1}$, $\vec{\Delta k} = \vec{k}_{up} - \vec{k}_p - \vec{k}_{IR}$), where $\vec{\Delta k}$ is a measure of the phase-mismatch amongst the three interacting waves. Under perfect phase-matching (PM) condition, the *upconversion efficiency* (η) reaches its maximum value. From the first proposal in 1968 [14] to the field deployable UCD in 2012 [2], the η has improved by six orders of magnitude even facilitating single photon detection. In general, an optically transparent nonlinear material is preferred for the UCD (e.g. $KTiOPO_4$ for 0.5 ~3.3 μm range, $LiNbO_3$ for 0.4 ~5.0 μm, $AgGaS_2$ up to 11 μm). However, if operating close to the absorption edge of the material, the influence of absorption and consequently the associated Planck radiation becomes the dominating noise source. From the thermodynamics of a black-body it is known, that if an object in thermal equilibrium (i.e. at a constant temperature) absorbs electromagnetic radiation, it also emits the same amount of radiation according to Kirchhoff's radiation law [20]. If this unwanted IR radiation satisfies the PM condition for upconversion, it contributes as thermal noise to the upconverted signal. At room temperature, this noise source is more pronounced in the MIR range in comparison to the UV-vis-NIR region as a consequence of the spectral distribution of black-body radiation. Few investigations of thermal noise contribution to the upconverted signal have been reported in the 1970's; one using a proustite crystal at room temperature [21] and a second using a $LiNbO_3$ crystal at 600 K [22]. In both cases, narrowband noise emission is considered in a relatively transparent region of the crystals (e.g. absorption coefficient = 0.22 cm^{-1} [21]). Comparing these initial results of the thermal noise contribution to a state-of-the-art UCD module, where the efficiency, η is 5 to 6 orders of magnitude higher and phase matches over a broad wavelength range, covering the absorption edge of the material, it is very important to include this thermal noise component in the analysis of the noise in the system. In recent years, the detection sensitivity has been improved to allow for MIR single photon counting [23]; however, still restricted to narrowband or pulsed applications. Thus, while the UCD technology is moving further into the MIR at room temperature and with broadband operation, it has now become extremely important to include thermally induced radiation in the UCD performance study in order to quantify the limits of the noise equivalent power in broadband UCDs.

$LiNbO_3$ is the most popular nonlinear material for applications, such as OPO, SFG, DFG, SHG, in the 2 - 5 μm regime. Though it is used for operation up to ~5 μm range, its optical transmittance at long wavelength falls off above 3.6 μm [24]. In this article, we consider an MgO doped periodically poled $LiNbO_3$ (PPLN) based intracavity UCD, where the spectral acceptance bandwidth covers the entire absorption edge of PPLN (3.5 – 5 μm). We first study the effect of absorption loss on the η and then we develop a rigorous model to quantify the thermal radiation contribution to the UCDs output when close to the absorption edge of the crystal. To the best of our knowledge, this is the first analysis and experimental demonstration of the internal thermal contribution in a highly efficient, broadband upconversion system with a quantification of the upconverted thermal radiation power when operated at room temperature or above.

2. Upconversion setup

A schematic diagram of the UCD module is shown in Fig. 1. A high finesse, CW, diode pumped (4W, 808 nm) solid state (Nd:YVO_4) laser at 1064 nm (TEM_{00}) is used as an intracavity upconversion system. All the cavity mirrors (M_1 – M_7) are HR-coated for 1064 nm and AR-coated for 700-900 nm, and M_7 is additionally HT-coated for the MIR light. For further details about the intracavity setup, see Ref [17]. A hot soldering iron rod at 400°C, emitting broadband black-body radiation, is employed as MIR input. The MIR light is phase-matched with the 1064 nm pump (beam radius of 180 μm, circulating power of 30 W) in a 20 mm long PPLN (AR coated for pump, IR and the upconverted waves, supplied by Covesion). The poling period is Λ = 23 μm and the aperture size is 1 mm × 1 mm. The PPLN is mounted in a Covesion supplied oven. The MIR light is focused into the PPLN using a CaF_2 lens (f_2,

Optics EXPRESS

50 mm, AR coated for 2 - 5 µm). The upconverted light is collimated by a silica lens (f_3, 75 mm, AR coated for 650 – 1050 nm). A short-pass 1000 nm (FS1000) and a long-pass 750 nm (FL750) filter is inserted to block the 1064 nm pump and 532 nm parasitic second harmonic light, respectively. Additionally, a long-pass 850 nm filter (FL850) is placed with a carefully tilted angle in the path of the collimated output beam to filter out residual diode power at 808 nm and to allow the upconverted light (820 ~880 nm) to pass (discussed in more detail in a later section). The upconverted signal is analyzed by a grating based spectrometer combining the UCD module and a NIR grating [25]. The upconverted light is collected and dispersed by a flat-field concave grating (Hiroba Jobin Yvon, Type IV, blank dimension: 46 × 46 mm^2, 595 lines/mm) and detected by a Si-IDS camera (801 × 801 effective pixel, 12-bit) for measuring the spectrum (Fig. 1). The position A in Fig. 1 is the location of virtual entrance slit (60 µm) for the grating, whereas position B is the plane of the flat-field dispersed spectrum produced by the grating (optical resolution in the MIR is ~20 nm). We have placed a highly sensitive Si-photodetector (Thorlabs, PDF10A) at position A to directly measure the upconverted power or similarly a Si-camera at position B to measure the spectrum. The entire configuration is compact and with minimal optics involved. In Fig. 2(a), the absorption spectrum of MgO-$LiNbO_3$ [24] is plotted, which clearly shows the long wavelength absorption edge starting at ~3.6 µm. In Fig. 2(b), the measured upconverted spectrum is plotted (blue solid curve) with detected NIR and the corresponding MIR wavelengths as x-axis. To identify the reason for non-uniform response of the UCD over the entire bandwidth, we have developed a numerical model that solves the coupled nonlinear equations for sum frequency generation [26] (CW case) using MATLAB®. It calculates the η including depletion, transmission loss thorough the PPLN (according to Fig. 2(a)), detector response of the Si-IDS, and the presence of atmospheric CO_2 absorption (in the path of 20 cm between the MIR source and UCD module, see Fig. 1). The calculated η is plotted in Fig. 2(b) as the red dashed curve, which qualitatively correlates well with the experimental spectrum (blue solid). To further illustrate the impact of the material absorption, we have also simulated and plotted the η in Fig. 2(b) for two additional cases, (i) for higher loss (1.5 × α, black dashed) and (ii) for α = 0 (green dashed). The study reveals that the absorption loss in PPLN is the dominating factor for determining the shape of the spectrum when close to the absorption edge. Note that, the exact absorption spectrum of the PPLN may well vary from the spectrum reported in Ref [24].

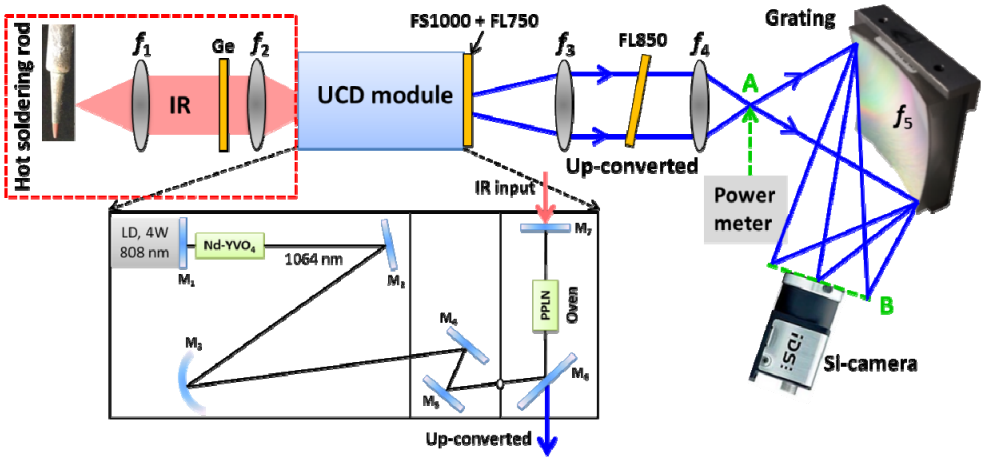

Fig. 1. Schematic diagram of the UCD module including a home build grating spectrometer. The upconverted spectrum is recorded by the Si-IDS camera at position B. The total power is recorded by a Si-photodetector at position A. The part surrounded by red-dashed box is the infrared input side, which has been removed during the noise measurement.

Optics EXPRESS

In addition to the reduced conversion efficiency, this strong absorption also results in thermal radiation added to the upconverted signal. The following sections are devoted to a rigorous analysis of this internal thermal radiation in PPLN based broadband MIR-UCD modules.

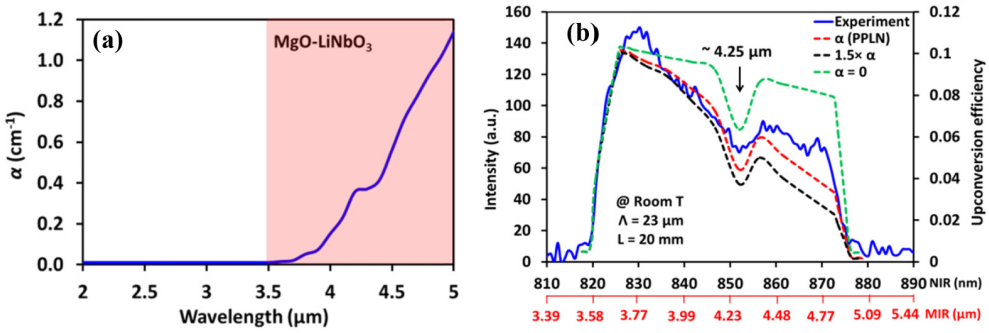

Fig. 2. (a) Optical power absorption coefficient (α) of MgO-LiNbO$_3$ for an e-polarized ray (Ref [24].). The shaded region is the working range of the UCD. (b) Measured upconverted spectrum of the hot soldering rod at 400°C (blue solid) and the theoretically calculated spectrum for three different absorption loss, α (red dashed), 1.5 × α (black dashed), and $\alpha = 0$ (green dashed). The small dip at 4.25 μm is due to the atmospheric CO_2 absorption.

3. Theoretical analysis of the thermal radiation

3.1 Modelling

In this section, we develop the model for calculating the generated optical power due to upconversion of thermal radiation in the PPLN crystal over the 3.5 – 5 μm range. We first consider the situation without external MIR input radiation to the UCD module (the part indicated by red dashed box in Fig. 1 is disconnected) and that only extra-ordinary polarization of the thermally radiated IR signal contributes to the upconversion process [17]. Thus this is the internal thermal radiation produced by the PPLN-UCD. The calculation steps follow the line of [21], however, additionally including the absorption loss in three wave mixing process and also calculating the upconverted power spectral density. The calculation steps are as follows:

(i) Calculate the IR radiation generated at the equilibrium temperature (T), emitted from a small slab of width dz at position z- within the PPLN (Fig. 3)

(ii) Express the IR radiation (dI_{IR}) emitted over a solid angle $d\Omega$ and IR wavelength range $d\lambda_{IR}$ in a range near the phase-matching wavelength λ_{IR}

(iii) Calculate the upconverted signal from dI_{IR}, including absorption loss in the three wave mixing process along the path inside PPLN

(iv) Calculate the total upconverted thermal radiation power as a superposition of upconverted thermal radiation contributions generated over the entire length of the crystal (L)

Optics EXPRESS

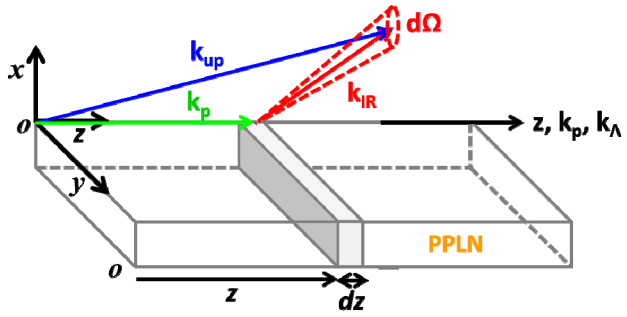

Fig. 3. Schematic diagram of the propagating wave vectors (k_{up}, k_p, k_{IR}) and the coordinate axes (x, y, z) used in the model. The pump beam and PPLN poling periodicity (wave vector is k_Λ) is along the *z*-axis.

Using polar coordinates, the emitted IR radiation from a slab of thickness *dz* inside the crystal over a solid angle $d\Omega$ and wavelength range $d\lambda_{IR}$ can be calculated from the Planck's radiation law as follows

$$dI_{IR}(T) = \frac{hc^2 n_{IR}^2 \alpha(\lambda_{IR})}{\lambda_{IR}^5 \left[\exp\left(\frac{hc}{\lambda_{IR} k_B T}\right) - 1\right]} dz \cdot d\lambda_{IR} \cdot d\Omega \qquad (1)$$

where k_B is Boltzmann's constant, *h* is Planck's constant, *c* is the speed of light in vacuum, n_m (for m = p, IR, up) is the refractive indices of the pump, IR and upconverted beam respectively inside the PPLN. The $\alpha(\lambda_{IR})$ is the wavelength dependent power absorption coefficient of the PPLN from Fig. 2(a) and *T* is the temperature of the crystal in Kelvin. Considering θ_{IR} as the angle between the IR wave and the *z*-axis, and φ_{IR} as the azimuthal angle, we can formally replace $d\Omega$ by $d\Omega = \sin\theta_{IR} d\theta_{IR} d\varphi_{IR}$. Considering plane wave approximation and re-absorption of the thermally generated IR radiation (during nonlinear interaction) along the path inside the PPLN, the upconverted power at the end of the nonlinear crystal can be expressed as [26],

$$dP_{up} = \left(\frac{8\pi^2 d_{eff}^2 P_p L^2 Z_0}{n_{up} n_{IR} n_p \lambda_{up}^2}\right)\left(\frac{L-z}{L}\right)^2 \left[\frac{\sinh^2\left(\frac{\alpha(\lambda_{IR})(L-z)}{4}\right) + \sin^2\left(\frac{\Delta k(L-z)}{2}\right)}{\left(\frac{\alpha(\lambda_{IR})(L-z)}{4}\right)^2 + \left(\frac{\Delta k(L-z)}{2}\right)^2}\right] e^{\left(\frac{-\alpha(\lambda_{IR})(L-z)}{2}\right)} dI_{IR} \qquad (2)$$

where d_{eff} is the effective nonlinear coefficient (~14 pm/V for PPLN), P_p is the pump power, *L* is the crystal length, Z_0 is the free space impedance, Δk is the phase-mismatch for the quasi PM condition ($k_{up} - k_p - k_{IR} - k_\Lambda$), and k_Λ is the grating vector along *z*-axis for the PPLN assuming a fixed poling period, Λ. In Eq. (2), the re-absorption loss $\alpha(\lambda_{IR})$ is only considered for the IR wave. Note that, we assume perfect PM in the transverse plane (i.e., $\frac{\sin\theta_{IR}}{\lambda_{IR}} = \frac{\sin\theta_{up}}{\lambda_{up}}$) and only the longitudinal phase-mismatch contributes to Δk.

Combining Eq. (1) and Eq. (2), we can calculate the *total upconverted thermal radiation power* by integrating Eq. (2) w.r.t. angles (θ_{IR}, φ_{IR}), wavelength (λ_{IR}) and length (*z*). In our case, the UCD module is optimized for a broad spectral acceptance bandwidth, 3.5 - 5 μm. Thus, it is relevant to calculate the *upconverted thermal radiation power spectral density*

Optics EXPRESS

($P_{thermal}^{up}$). Therefore we exclude the λ_{IR} integration and calculated the power spectral density as follows:

$$P_{thermal}^{up}(\lambda_{IR},T)=\frac{hc^2\alpha(\lambda_{IR})}{\lambda_{IR}^5\left[\exp\left(\frac{hc}{\lambda_{IR}k_BT}\right)-1\right]}\left(\frac{8\pi^2d_{eff}^2P_pL^2Z_0}{\lambda_{up}^2}\right)\times$$
$$\int_z\int_{\varphi_{IR}}\int_{\theta_{IR}}\left[\left(\frac{n_{IR}}{n_{up}n_p}\right)\left(\frac{L-z}{L}\right)^2e^{\left(\frac{-\alpha(\lambda_{IR})(L-z)}{2}\right)}\left\{\frac{\sin h^2\left(\frac{\alpha(\lambda_{IR})(L-z)}{4}\right)+\sin^2\left(\frac{\Delta k(L-z)}{2}\right)}{\left(\frac{\alpha(\lambda_{IR})(L-z)}{4}\right)^2+\left(\frac{\Delta k(L-z)}{2}\right)^2}\right\}\right]\sin\theta_{IR}\,d\theta_{IR}\,d\varphi_{IR}\,dz \quad (3)$$

We have assumed azimuthal symmetry for the upconversion process by integrating Eq. (3) for φ_{IR} over a 0 - 2π angle. The temperature and wavelength dependent Sellmeier equation [27] is used in the refractive index calculation. Since we consider non-collinear interaction among the participating waves (see Fig. 3), the angular dependent refractive index is also included as all the waves are extra-ordinarily polarized [3]. Thus Δk depends on the angle between the interacting waves (θ and φ). The argument of "sin" function in Eq. (3) is the primary factor for determining the upconverted spectral bandwidth and acceptance angle (range of θ_{IR} and φ_{IR}). At the end, the total thermal radiation power is calculated by integrating the power spectral density with respect to wavelength using trapezoidal rule.

3.2 Numerical results

A 20 mm long PPLN with a poling period, Λ = 23 μm is considered for the numerical simulation. An improved setup for the noise study with 60 W of intracavity power at 1064 nm is considered; keeping all other parameters the same as used in the previous measurement (corresponds to Fig. 2(b)). The thermal effect is studied over a temperature (T) range of 20 – 200°C, which is the typical temperature range for the nonlinear material. First we calculate the perfect black-body (emissivity = 1) radiation spectrum for T = 40°C, 80°C, 120°C, 140°C, 160°C and 200°C, and then plot the corresponding spectral radiance over the 3.5 – 5 μm range, see solid curves in Fig. 4(a). The actual emission spectrum of the PPLN (at L = 20 mm) is then simulated by multiplying the spectral dependent emissivity of the PPLN to the perfect black-body radiance curve, see dashed curve in Fig. 4(a). Different colors correspond to different temperatures as indicated at the right side of the plot. The η of the UCD module for different operating temperatures of the PPLN is computed for non-collinear PM under ideal condition (assuming no crystal loss); see Fig. 4(b). Note that η is plotted for MIR light propagating with non-collinear PM input angles (see [17] for details). The PM bandwidth of the UCD setup is widest at room temperature, and it gradually decreases for higher temperature depending on the PM condition. The next step is to calculate the upconverted thermal radiation power spectral density for different temperature using Eq. (3). The result is plotted in Fig. 4(c).

Optics EXPRESS

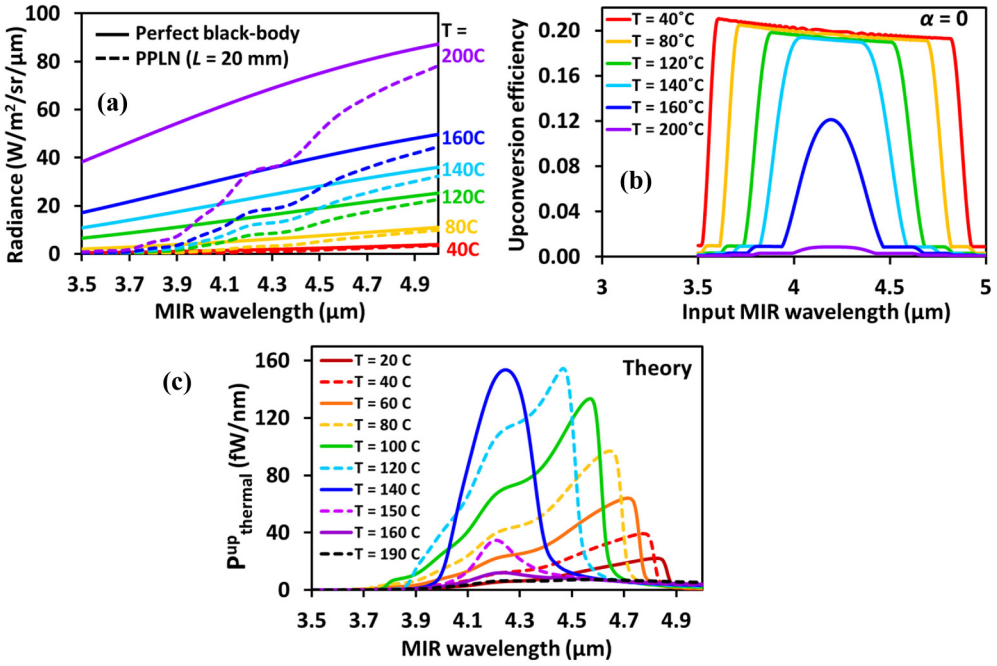

Fig. 4. Numerically simulated (a) spectral radiance of perfect black-body (solid curves) and non-transparent PPLN (dashed curves), (b) upconversion efficiency of the UCD module (ideal loss-less case), and (c) upconverted thermal radiation power spectral density for the proposed UCD for different temperatures.

As expected, at lower temperatures of the crystal, the spectral bandwidth of the thermal radiation is higher and the peak of the spectrum is closer to the longer wavelength (absorption) edge when compared to the corresponding graphs of Fig. 4(b). The shape of the curve follows the trend of the black-body spectrum (see Fig. 4(a)). With increasing temperature, the peak value of the power increases according to Fig. 4(a) (dashed curves); however, its position shifts towards the center of the PM bandwidth (Fig. 4(b)). The overall spectral bandwidth becomes narrower following the PM curves of Fig. 4(b). For T > 140°C, η decreases drastically as expected from Fig. 4(b), which clearly influences the upconverted thermal power. In Fig. 4(c), the small hump in all the curves (clearly visible for T < 140°C) around 4.2 μm wavelength, is the signature originating from the absorption curve of PPLN (see Fig. 2(a)), extracted from the Ref [24].

4. Experimental verification

To validate the numerical calculations, we have conducted an experiment with a setup similar to that shown in Fig. 1. The intracavity 1064 nm laser is used as pump beam with approximately 180 μm beam waist radius inside the PPLN. First, the whole setup is aligned including the grating and Si-camera, using a hot soldering iron rod as MIR input to the UCD module. After alignment, the MIR input (the part indicated by red-dashed box in Fig. 1) is removed and an external thermal power meter is placed just behind mirror M_7 (see the inset of Fig. 1) to monitor the intracavity power at 1064 nm (i.e. the leakage laser power). The noise measurement is conducted in a setup with the upconversion side shielded from ambient light. Throughout the entire experiment, the camera integration time is fixed at 800 ms and the power at 1064 nm is recorded for each measurement. Note that, all of the graphs of the detected spectrum are plotted with the MIR wavelength as the x-axis. The experimental setup used for the measurement of the upconverted thermal radiation spectrum is shown in Fig. 5(a). Before placing the FL850 filter between the two lenses (f_3 and f_4), we have first nulled

Optics EXPRESS

all the contributions from background/stray light (see Fig. 5(b)) and subsequently measured the spectrum for different diode laser (LD) currents (I = 0 to 3A) while keeping the PPLN at room temperature. The rest of the measurement is realized at a fixed LD current (3A). We noticed that the primary noise contribution is coming from the unfiltered LD. To block the residual light from the LD, we placed the FL850 filter (Fig. 5(a)) and tilted it precisely (without disturbing the setup) just to block the pump band without blocking the upconverted signal (see Fig. 6(a)). We continued the noise study keeping the FL850 in that position.

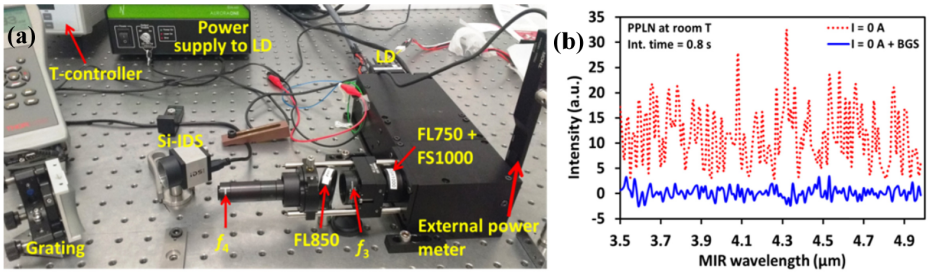

Fig. 5. (a) Experimental setup used for measurement of the upconverted thermal radiation spectrum using a concave grating dispersed Si-camera, coupled with the upconversion module. (b) Recorded spectrum before (red dotted) and after (blue solid) camera background subtraction (BGS) at room temperature for zero LD current.

In the next step, we change stepwise the PPLN temperature while keeping the LD current constant at 3A and measure the upconverted thermal radiation spectrum. It is observed that for different temperatures, the intracavity laser power varies owing to changes in the laser cavity. Thus, we continuously monitor the leakage power while performing the measurements and each spectrum is calibrated for an intracavity pump power of 60 W. For accuracy, we have calibrated the temperature reading of the temperature controller (Thorlabs) beforehand by measuring the temperature of the PPLN (while mounted in the oven) using an external thermocouple. For the rest of the plots, we use calibrated temperatures. The PPLN is heated from room-temperature to as high as 170°C while the upconverted spectrum is recorded (Fig. 6(b)). For each measurement, the temperature is allowed to stabilize for at least 10 min. The theoretical spectrum (Fig. 4(c)) and the experimentally measured spectrum (Fig. 6(b)) show similar trends as a function of temperature.

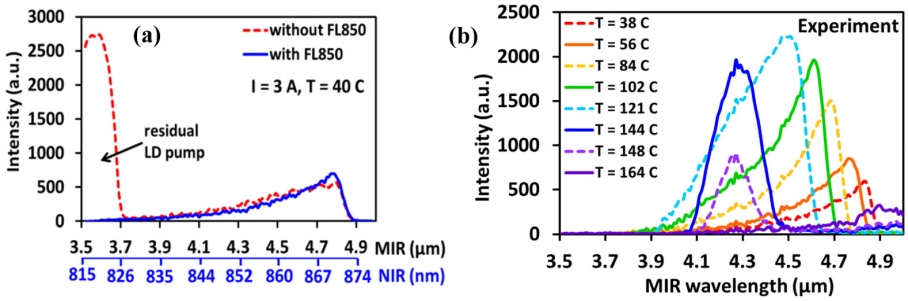

Fig. 6. Experimentally measured upconverted thermal radiation spectrums at integration time of 800 ms. (a) Result with (blue solid) and without (red dashed) the FL850 filter for a LD current of 3A. Both MIR and NIR scale is used as *x*-axis for easy identification. (b) Spectrum at different temperature of PPLN for a constant intracavity power of 60 W.

5. Absolute power: comparison between theory and experiment

Furthermore, we have directly measured the total power using a highly sensitive femto-watt Si-photodetector. We have placed the detector at the focal plane of the lens f_4 (position A in Fig. 1). The detector is mounted on a 3-D translational stage for accurate positioning. The

Optics EXPRESS

output voltage is measured by an oscilloscope. Two additional filters, long-pass 800 nm (FL800) and short-pass 900 nm (FS900), are mounted at the input of the detector to block any stray light. Moreover, a ND1.0 filter is used to exploit the full dynamic range of the photodetector. The total upconverted thermal radiation power at different temperatures is plotted in Fig. 7 (blue circled). We have subtracted the dark noise (detected power at zero LD current) while plotting this graph. Approx. 30 pW of thermal radiation power is measured at room temperature and a maximum of ~70 pW at 120°C is recorded for the broadband PPLN-UCD. To validate the proposed theory, we have calculated the total upconverted thermal radiation power by integrating the modeled power spectral density for the corresponding temperature (Fig. 4(c)); see Fig. 7 (red dashed curve, Theory_int.). The qualitative similarity in the two curves reveals that the complex numerical simulation agrees well with the experimentally recorded value.

However, quantitatively there is a clear offset between the two curves. So far we assume no MIR input to the UCD module. However in the experiment, a thermal source (power meter for calibration of the intracavity power) is placed right in front of the input side of the UCD, see Fig. 5(a). It is at ambient temperature, and emits thermal radiation according to Kirchhoff's radiation law. The body material of the detector is black anodized aluminum, whose emissivity is around 0.77 at 300 K [28]. We have calculated the contribution to the upconverted noise power due to this external source at constant ambient temperature of 20°C; see red dotted curve in Fig. 7. The external contribution decreases with increasing temperature of the PPLN, following the decreasing PM bandwidth of the UCD module. Furthermore, we have plotted the numerical sum of the two thermal contributions (internal and external) as the total thermal radiation of the PPLN-UCD under investigation, see red solid curve in Fig. 7. The experimental data (blue circled) not only qualitatively, but also *quantitatively* matches quite well with the numerical analysis (red solid) even at that 10's of pW power level. In comparison to Fig. 4(c), we observe an increase in the power level of the radiation spectrum in Fig. 6(b) at the long wavelength edge (around 5 μm) for higher temperature (> 150°C). We speculate that this may be arising from higher order or Type-II phase matching taking place in the upconverter at higher temperatures in combination with a sub pW level contribution from the PPLN-oven material over the detected spectral range. The offset of ~10 pW between the tails of the theoretical and experimental curves in Fig. 7 is probably coming from this phenomenon. Finally, we have also calculated the upconverted SPDC power level for our setup to identify any other competitive noise contribution. It shows that the SPDC contribution is < 1% of the detected thermal radiation power in the considered wavelength range.

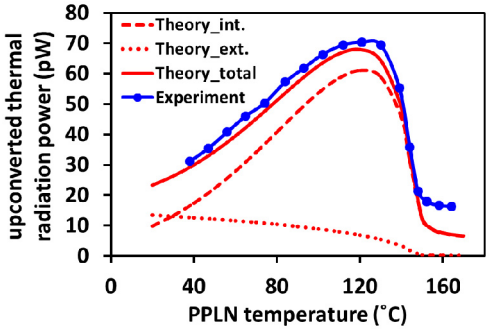

Fig. 7. Direct power measurement of the upconverted thermal radiation (blue circular spot) for intracavity pump power of 60 W. The red curves are theoretically calculated absolute power for similar experimental conditions. Red dashed and red dotted correspond to the internal contribution (PPLN as the thermal source) and external contribution (MIR coming from input side), respectively. Red solid is the combined plot (internal + external).

Optics EXPRESS

6. Conclusion

In conclusion, we have developed a numerical approach to quantify the contribution of internal thermal radiation in a broadband frequency upconversion detector (UCD). Thermal light, originating from black-body radiation of the semi-transparent nonlinear material itself, dominates the noise in a highly sensitive UCD when operating at the optical absorption edge of the nonlinear material. Thermal effect becomes severe even at room temperature, when operating in the MIR spectral range. In state-of-the-art UCD technology, where research is moving further into the MIR domain including broadband coverage and ultra-high sensitivity, the choice of appropriate nonlinear material and the quantification of the upconverted thermal radiation power becomes of prime importance. Towards meeting these goals, we have calculated and experimentally measured – for the first time to our knowledge – the upconverted internal thermal radiation spectrum as well as the absolute upconverted thermal radiation power of a bulk PPLN-based, broadband, highly efficient UCD covering the functional group regime, 3.5 – 5 μm. We have developed a compact in-house upconversion spectrometer, combining a CW intracavity upconverter followed by an aberration corrected flat-field concave grating and a cost effective Si-IDS camera, to detect the spectrum. Secondly, a femto-watt Si-photodetector is used to directly measure the upconverted power. All the measurements are carried out from room temperature to around 200°C, which is typically used for $LiNbO_3$ based applications. In case of a 20 mm long PPLN an absolute upconverted thermal radiation power of ~30 pW at room temperature and ~70 pW at 120°C are detected at 60 W of circulating CW pump power. The experimental results agree well both qualitatively and quantitatively with the model. The detected total power (blue dots in Fig. 7) matches well with the calculated one (red dashed in Fig. 7), which is simulated by integrating the theoretical (optical) power spectral density (Fig. 4(c)). Thus, we may likely conclude that, the Fig. 4(c) (and/or Eq. (3) can be used to estimate the internal thermal radiation power spectral density of the UCD system. In the proposed UCD, while operating at the absorption edge of the $LiNbO_3$, the contribution from upconverted SPDC noise becomes negligible comparing to the thermal noise (<1%). We note that from the measured total upconverted internal thermal radiation power (Fig. 7) we can estimate the noise at room temperature to be ≈3.8 fW/Hz$^{1/2}$. Since $LiNbO_3$ is the most popular nonlinear material for many applications (OPO, DFG, SFG, SHG etc.) up to 5 μm, we believe that this detailed model will make a significant contribution to the $LiNbO_3$ research community. Furthermore, this model can be useful for the investigation of thermal noise in other nonlinear materials used for UCDs.

Funding

Innovation Fund Denmark (4107-00011A).

Acknowledgment.

We thank Finn A. C. Pedersen for helping with the electrical connections, Dr. Peter J. Rodrigo for useful discussion on filter and for lending the femto-watt power meter, Dr. Lasse Høgstedt of NLIR for technical discussion in lab, and Lichun Meng for useful discussion on SPDC noise.